JOURNAL OF MATERIALS SCIENCE 27 (1992) 6159–6170

Effect of precipitate type and morphology on high-temperature creep and internal stress in Al–Li based alloys

C. K. L. DAVIES, S. POOLAY-MOOTIEN*, R. N. STEVENS
Materials Department, Queen Mary and Westfield College, University of London, Mile End Road, London E1 4NS, UK

The tensile creep of a series of aluminium–lithium-based alloys, two binary alloys containing δ′ precipitate, and the 2090 alloy containing δ′ and T_1 precipitate, has been studied over a range of stresses at 150 °C. In some cases the internal stress developed during creep has been determined using the strain transient dip test. The results have been compared with similar data previously obtained for the 8090 alloy containing δ′ and S precipitates. The solid solution alloy and the binary alloy containing shearable δ′ particles exhibited normal Class II behaviour, with the development of sub-grains and a stress dependence of the creep rate given by a single stress exponent, *n*, between 4 and 5 at all applied stresses. The alloys containing particles not easily sheared by dislocations, coarse δ′, S and T_1, exhibited similar stress dependencies of the creep rate at low stresses but exhibited large values of *n*, between 18 and 35 at high stresses. The internal stress, σ_i, in these alloys was found to be approximately constant at high stresses possibly due to partial shearing of the coarse δ′, T_1, and the S on sub-boundaries. The stress dependence of the minimum creep rate, $\dot{\varepsilon}$, could be represented at all applied stresses, σ_a, by $\dot{\varepsilon} \propto (\sigma_a - \sigma_i)^n$, where $(\sigma_a - \sigma_i)$ is the effective stress driving dislocations during creep, and *n* is a single stress exponent of between 5 and 6 for all applied stresses. The internal stress, which increases with applied stress, at least at a low applied stress, arises from inhomogeneity of plastic deformation, due to hard sub-boundaries or hard particles which are Orowan looped. These two types of contribution to the internal stress are of similar magnitude in the alloys containing coarse δ′ and T_1 but the majority of the internal stress in the 8090 alloy may arise as a result of the hardening of sub-boundaries by the S precipitate.

1. Introduction

Particle-hardened nickel-based alloys exhibit, at least at high stresses, a very high stress dependence of the minimum creep rate and unrealistically high apparent creep activation energies [1–6]. A similar behaviour has been found for the commercial 8090 Al–Li alloy containing δ′ and S precipitates [7–9]. In this case, the stress dependence of the minimum creep rate, $\dot{\varepsilon}$, could be described by $\dot{\varepsilon} = A\sigma_a^n$, where σ_a is the applied stress, with the stress exponent *n* being around 4–6 at low stresses and 30–40 at high stresses. The similarity of behaviour was thought to be related to the fact that nickel-based alloys are hardened by the coherent precipitate γ′ (Ni_3Al) which is isomorphous with the δ′ (Al_3Li) found in Al–Li alloys.

It has been suggested, for both nickel-based alloys [1–6] and for 8090 [8, 9] that these high stress dependencies arise from the fact that creep is driven by the effective stress $(\sigma_a - \sigma_o)$ rather than by the applied stress. Furthermore it has been demonstrated that σ_o can be approximated to an internal stress, σ_i [5, 6, 9] as determined by the strain transient dip test [10]. Such measurements for Nimonic 91 [5, 6] and 8090 [9] showed the internal stress to increase linearly with applied stress at low creep stresses and become approximately constant at high creep stresses. As a result the minimum creep rate was found to be a simple function of the effective stress $(\sigma_a - \sigma_i)$ with a stress exponent, *n*, of between 5 and 6 at all applied stresses.

In the case of Nimonic 91, the internal stress measured at low creep stresses correlated well with the internal stress calculated from the observed density of Orowan loops around γ′ particles [5, 6]. It was suggested that the internal stress increased with applied stress at low creep stresses, as a result of the increasing loop density, but becomes constant at high stresses as the γ′ particles were sheared or partly sheared by dislocations.

In the case of 8090 the situation was by no means so clear. The alloy contained the rod-like S (Al_2CuMg)

Permanent address: University Aix-Marseille II, France.

0022–2461

precipitate in addition to δ′. Furthermore, a well-developed system of sub-grains was present. Stable Orowan loops have been observed in Al–Li alloys up to temperatures of 493 K [11] and dislocation loops were observed after creep in the 8090 alloy [9]. However, whether the loops were around δ′ or S was unclear. It is likely that S is looped at all but the highest stresses, as it is not easily sheared by matrix dislocations gliding on {1 1 1} planes. However, whether δ′ is looped or not depends on the δ′ particle size and volume fraction. Furthermore, the particle size at which δ′ looping occurs is certainly affected by the presence of S. The fact that some dislocation pairs were seen suggested that δ′ was sheared by matrix dislocations. It is possible then that it is the loops around S which are, at least in part, responsible for the measured internal stress, and that it is the shearing of S at high stresses which results in the constancy of the internal stress. If this is the case, then while the rationale for the high stress dependence of the creep rate in 8090 is similar to that for Nimonic 91 it is not the case that in 8090, δ′ plays an identical role to γ′ in Nimonic 91.

It can be seen from the above that while the role of Orowan loops around γ′ in Nimonic 91 in determining the internal stress and yielding the high stress dependence of the creep rate is clear, the situation for 8090 is by no means so clear. It was hence decided to investigate the effect of precipitate size and morphology on the stress dependence of the creep rate and the internal stress in a series of Al–Li–X alloys. Three binary Al–Li alloys were prepared and heat treated such that one was a solid solution, one contained fine δ′ which was sheared by matrix dislocations and one contained coarse δ′ which was Orowan looped. These were compared with an Al–Li–Cu, 2090 alloy heat treated to yield very fine δ′, which was sheared by matrix dislocations, but which also contained T_1 (Al_2CuLi) plates which were not expected to be cut easily, hence yielding dislocation loops. The results from these four alloys were to be compared with the previous results for the 8090, containing δ′ and S precipitates. It was hoped to determine the relative roles of looping of precipitate particles, whether δ′, T_1 or S, and the dislocation sub-grain walls in determining the magnitude of the internal stress and hence in determining the stress dependence of the creep rate.

2. Experimental procedure

Three binary Al–Li alloys were supplied as cast ingots which where subsequently hot rolled at 803 K to 1 cm thick slabs. The initial lithium contents are given in Table I together with the final lithium contents, following fabrication and heat treatment. The heat treatments given to the alloys are listed in Table II. These are the result of considerable experimentation in order to produce the desired δ′ particle size.

The 2090 alloy was supplied in the form of hot-rolled slab and the composition is given in Table III, together with the composition of the 8090 previously studied [9]. The heat treatments given to both alloys are also shown in Table IV.

Cylindrical creep specimens with threaded ends, 25.4 mm gauge length and of diameter 4.50 mm, were machined from the hot-rolled plates. Constant stress tensile creep tests were performed in air at a temperature of 423 K as described previously [9], as were strain transient dip tests [9, 10].

Some tensile tests were carried out at 293 K, using either an Instron 1195 machine at a strain rate of $3 \times 10^{-4}\ s^{-1}$, or by direct loading using the creep machines. These tests were carried out on specimens heat treated in a variety of ways in order to produce the required δ′ particle size.

For the purpose of dislocation and precipitate structure characterization, thin foils were prepared for transmission electron microscopy (TEM) as described previously [9]. The foils were examined in a Jeol 100CX transmission electron microscope using, bright-field (BF), two-beam bright-field (TBBF), centred dark-field (CDF), and weak-beam imaging modes. Film thicknesses were measured using a convergent beam technique [12, 13].

3. Results and discussion

3.1. Initial dislocation and precipitate structure of the alloys

It was essential for this study to produce well-characterized structures in which it was certain that particles

TABLE I

Alloy	Initial mass % Li	Final mass % Li	Volume fraction δ′ from phase diagram [15]	Measured volume fraction δ′	δ′ particle radius (nm)
Al–1% Li	1.16	0.95 (3.57)	–	–	–
Al–2% Li	2.22	1.94 (7.09)	0.045	0.04 (0.048)	13.3 (12.5)
Al–3% Li	3.29	2.75 (9.84)	0.22	0.227 (0.37)	87 (75)

TABLE II

	Al–2% Li	Al–3% Li
Thermomechanical history	1. Cast ingot hot rolled at 803 K to 1 cm slab	Cast ingot hotrolled at 803 K to 1 cm slab
	2. Solution treated at 803 K for 30 min, water quenched to room temperature	Solution treated at 803 K for 30 min, water quenched to room temperature
	3. Aged at 463 K for 16 h	Aged at 463 K for 10 days

TABLE III

	Li (%)	Cu (%)	Mg (%)	Zr (%)	Al (%)
2090	1.99 (7.26)	2.57	–	0.11	Bal.
8090	2.3 (8.33)	1.2	0.67	0.13	Bal.

would either be sheared by dislocations or Orowan looped. Considerable experimentation was hence carried out to determine the appropriate heat treatments particularly for the 1.94 and 2.75 mass % Li binary alloys. The final heat treatments were chosen on the basis of the measured 0.2% tensile proof stress, the measured particle sizes and volume fractions, the theoretically calculated proof stresses based on cutting or looping and previous literature data. It was surprising that reference to literature data was not sufficient, but this revealed few examples of either identical lithium contents and/or similar heat-treatment temperatures. Furthermore, considerable uncertainty seems to exist as to exact volume fractions and exact particle sizes.

The three binary alloys exhibited equiaxed grains of average diameter 0.2 mm. No sub-grains were present prior to the deformation. The measured δ′ particle sizes and volume fractions, measured from electron micrographs (Fig. 1), are the values in parentheses given in Table I, together with the values corrected for the effect of foil thickness [14]. These compare very well with the estimates of the volume fraction made from the phase diagram [15], Table I. Uncorrected volume fraction data in the literature should be treated with caution, especially results that suggest that the volume fraction in binary alloys may increase from 1% to 10% during ageing [16]. At very small particle sizes results should be corrected for overlapping [17] and at larger particle sizes should be corrected for foil sectioning of particles [14, 17]. The only results found in the literature in which corrections of this type have been carried are those of Huang and Ardell [18] and Cassada *et al.* [19]. The present results have been corrected using the relationship [14]

$$f_a = f\left(1 + \frac{3\pi}{8}\frac{\overline{\rho^4}}{\overline{\rho^3}}\bar{R}\right) \quad (1)$$

where, f_a is the apparent volume fraction (found by dividing the total volume of particles per unit area of foil by the foil thickness), f is the true volume fraction, $\bar{R} = \bar{r}/t$ where $\bar{r}$ is the true mean particle radius and t is the foil thickness, ρ is the particle radius divided by the mean particle radius, and $\overline{\rho^4}$ and $\overline{\rho^3}$ are the mean

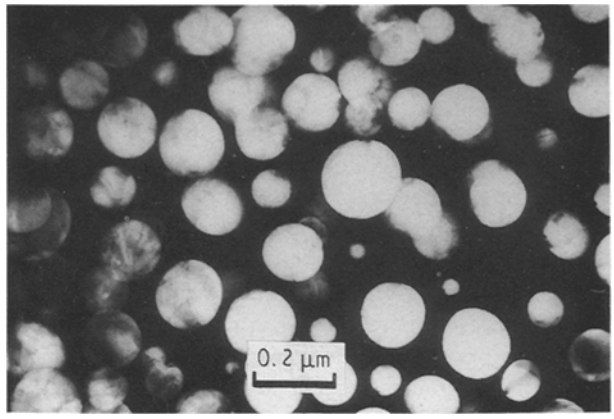

Figure 1 Centred dark-field transmission electron micrograph using {1 0 0} δ′ spot in Al–2.75% Li aged at 463 K for 10 days.

values of ρ^4 and ρ^3. The true mean particle radii have been calculated, assuming that particles are truncated by the foil surface, using the relationship

$$\frac{\bar{r}_a}{\bar{r}} = \left(1 + \frac{\pi}{2}\bar{R}\overline{\rho^2}\right)\Big/(1 + 2\bar{R}) \quad (2)$$

where $\bar{r}_a$ is the apparent mean radius.

If the δ′ particles are relatively large the increase in shear yield stress due to cutting is given by [17]

$$\Delta\tau_c = \frac{\gamma}{2b}\left[\left(\frac{4f}{\pi}\right)^{1/2} - f\right] \quad (3)$$

and that due to Orowan looping is given by [17]

$$\Delta\tau_o = \frac{0.813Gb}{2\pi(1-\nu)^{1/2}}\frac{\ln(2\bar{r}/r_c)}{\lambda - 2\bar{r}} \quad (4)$$

where γ is the anti phase boundary energy $\approx 0.15\ \mathrm{J\,m^{-2}}$ [20], b is the magnitude of the Burgers vector $= 0.286 \times 10^{-9}$ m $\approx r_c$ (dislocation core radius), G the shear modulus ≈ 30 GPa [21], ν is Poisson's ratio ≈ 0.34 [22, 23], and $\lambda = 1.23\bar{r}(2\pi/3f)^{1/2}$.

The calculated values are for the 1.94 mass % Li alloy $\Delta\tau_c = 48.6$ MPa and $\Delta\tau_o = 120$ MPa and for the 2.75 mass % Li alloy $\Delta\tau_c = 81.5$ MPa and $\Delta\tau_o = 58$ MPa. This strongly suggests that in these heat-treated conditions δ′ particles are cut in the 1.94% Li alloy and Orowan looped in the 2.75 mass % Li alloy. These values can be compared with the measured values of the 0.2% tensile proof stress, $\sigma_{0.2}$, of the alloys which were 158 and 218 MPa, respectively, for the 1.94% Li and 2.75% Li alloys. The value for the higher lithium content alloy must be treated with some caution as its very much higher work-hardening

TABLE IV

	2090	8090
Thermomechanical history	1. Cast ingot hotrolled at 803 K to 4.5 cm slab	Cast ingot hot rolled at 803 K to 4.5 cm slab
	2. Solution treated at 803 K for 30 min, water quenched to room temperature	Solution treated at 803 K for 30 min, water quenched to room temperature
	3. 2% plastic deformation followed by ageing at 463 K for 16 h	2% plastic deformation followed by ageing at 463 K for 16 h
	4. Reversion heat treatment at 538 K for 1 min, water quenched to room temperature	–

rate made determination of $\sigma_{0.2}$ more difficult. The first problem, however, is the correct value of the Taylor factor to be used. In the literature values of 2 [24], 2.5 [25], 3.1 [19, 20] and 3.33 [26] have been used for binary Al–Li alloys. It is proposed here to use the original Taylor value of 3.0 as there appears no outstanding evidence for anything else.

The second problem is the values to be used for the shear yield stress of the matrix (or the $\sigma_{0.2}$ of the matrix) for the appropriate lithium content for the given ageing temperature. Miura *et al.* [16] quote a value of approximately 10 MPa for the shear yield stress of Al–2.0 mass % Li single crystals quenched from 200 °C and 54.4 MPa for the shear yield stress of the alloy with a particle size of 13.3 nm. The calculated shear yield stress of our 1.94 mass % lithium alloy, assuming cutting, would hence be (48.6 + 10) MPa or 58.6 MPa comparing well with the value of Miura *et al.* already quoted. If a Taylor factor of 3.0 is used the calculated $\sigma_{0.2}$ would be 175.8 MPa. The current measured value is 158 MPa. This can be compared to the Sainfort and Guyot [24] value for $\sigma_{0.2}$, of 180 MPa for a particle size of 13.3 nm but with a considerably higher volume fraction of δ′. The reasonable agreement between the calculated shear stress values for δ′ shearing, the measured values of Miura *et al.* [16] and Sainfort and Guyot [24], and the present measure values, lend support to the case that δ′ is sheared by dislocations in the 1.94 mass % Li alloy heat treated as in Table II.

For the 2.75% Li alloy, if the value quoted by Miura *et al.* [16] for the matrix shear stress, of 10 MPa is also used, then the calculated shear yield stress would be (58 + 10) MPa or 68 MPa and the value of $\sigma_{0.2}$ would be 204 MPa, compared to the measured value of 218 MPa. Huang and Ardell [20] quote a range of values for the matrix yield stress of Al–Li binary alloys, most of which fall in the range 5–22 MPa with the only exceptions being the results of Noble *et al.* [26]. If a maximum value of 22 MPa is used then the calculated value of $\sigma_{0.2}$ would be (58 + 22) × 3 = 240 MPa. It is hence apparent that both the calculated and measured values of $\sigma_{0.2}$ support the contention that δ′ particles in the 2.75% Li are Orowan looped.

Transmission electron microscopy studies of the two alloys deformed at room temperature showed evidence of paired dislocations in the 1.94% Li alloy and extensive dislocation looping in the 2.75% Li alloy. Thus the combined evidence of the theoretical calculations, measured values of $\sigma_{0.2}$ and TEM observations confirm that heat treatments have been chosen which result in δ′ being cut in the 1.94% Li alloy and Orowan looped in the 2.75% Li alloy.

The 2090 alloy had equiaxed grains of 0.5 mm diameter containing a well-developed substructure with an average sub-grain size of 5 μm. The alloy was given a reversion heat treatment (Table IV) [18], in order to produce as fine a δ′ structure as possible, to ensure that δ′ was cut by matrix dislocations. Following this treatment, δ′ superlattice spots were not present in the electron diffraction pattern although these appeared subsequently in creep-tested specimens. The largest δ′ particles observed, after creep were of 2.5 nm radius. This maximum δ′ particle size was still well below the particle size for the transition from cutting to looping even in the presence of the T_1 phase [24]. This volume fraction of δ′ was estimated to be about 0.04 for the 1.99% Li, 2090 alloy. This is very similar to the value for the current binary alloy with an almost identical lithium content (1.94%). This is contrary to the results of Huang and Ardell [27] who suggested that the presence of the T_1 phase reduces the volume fraction of δ′ but agrees with the results of Sainfort [28] who found similar volume fractions independent of the presence of T_1 plates.

The alloy contained T_1 plates lying on {1 1 1} matrix planes in ⟨1 1 0⟩ matrix directions. The plates were approximately 2 nm thick and of length 100–150 nm (Fig. 2a, b) with the whole of space subdivided by the plates with frequent near-plate impingement. The development of T_1 plates in 2090 type alloys has been extensively studied although usually in alloys with larger lithium contents than the present (1.94 mass %) [24, 27–31]. Cassada *et al.* [30] found, for an Al–2.45 Li–2.45 Cu–0.18 Zr alloy, stretched 2% before ageing at 190 °C for 16 h (identical treatment to the present alloy without the reversion), T_1 plates of thickness 2 nm, 140–190 nm length, volume fraction 0.019 and number density of $7 \times 10^2\ \mu m^{-3}$, results which are very comparable with the present alloy in spite of the difference in the lithium content. The

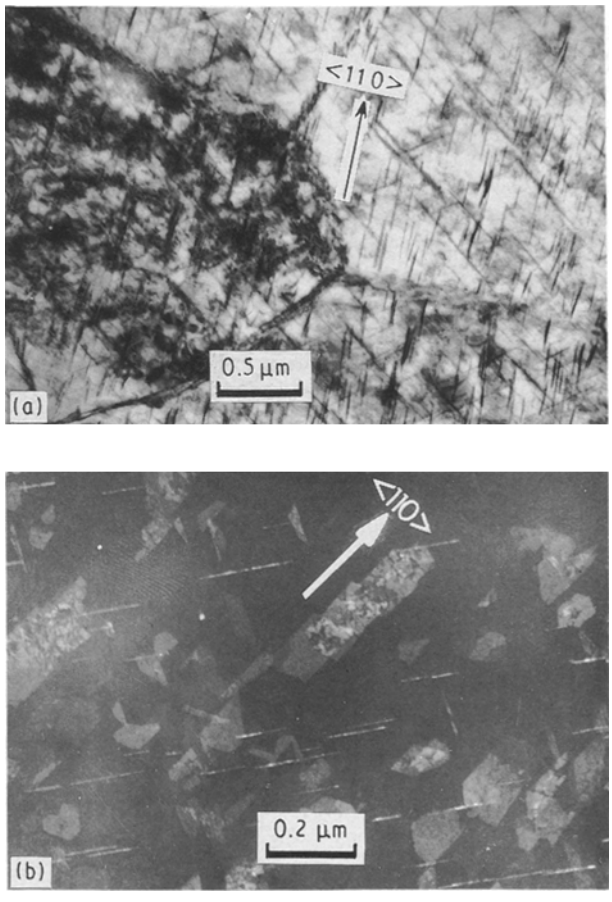

Figure 2 (a) Bright-field transmission electron micrograph showing sub-grains and edge-on T_1 plates in 2090. (b) Centred dark-field image transmission electron micrograph showing T_1 plates. B = ⟨1 1 2⟩.

present alloy, following the reversion treatment to dissolve the δ′, had a room-temperature $\sigma_{0.2}$ of 281 MPa. This compares very well with the value of 299 MPa measured by Huang and Ardell [18] after a similar treatment for a 2.85% Cu alloy. This yield stress results only from solid solution strengthening of the matrix and from the effect of the presence of the T_1 plates which cannot be easily sheared by {1 1 1} ⟨1 1 0⟩ matrix dislocations which must hence bypass or loop them [24]. The creep-tested specimens will, however, contain some very fine δ′ which will contribute to the flow stress.

The initial structure of the 8090 alloy has been reported previously [9] but is included here as the previously determined creep properties [9] are to be compared with the results for the present alloys. The alloy has pancake grains with a well-developed sub-grain structure of dimensions of approximately 20 μm. δ′ particles present are of 23 nm diameter and volume fraction of 0.05. The sub-grains are threaded with S laths lying along ⟨0 0 1⟩ matrix directions on {2 1 0} matrix planes (Fig. 3) and there is extensive precipitation of S on sub-grain boundaries (Fig. 4). The S laths are of approximately 5 nm diameter and 200 nm long with an initial volume fraction of 0.001, within the sub-grains. The spacing of S on sub-grain boundaries is smaller than within the grains and the local volume fraction seems higher. The δ′ particles of this size will be cut by matrix dislocations at the room-temperature yield stress but the orthorhombic S cannot easily be sheared by {1 1 1} ⟨1 1 0⟩ slip and will hence be looped.

3.2. Dislocation structure in creep-tested specimens

The solid solution alloy (1% Li) shows the formation of well-developed subgrains during creep (Fig. 5). The structures are similar to those observed in aluminium [32], Al–Mg alloys [33, 34] and Al–2% Li [35] when crept under conditions of climb control, as contrasted with the random arrays of curved dislocations seen when creep is controlled by viscous glide [33, 34]. The nominally 2% Li binary alloy also shows the development of sub-grains (Fig. 6) but the sub-grains are seen

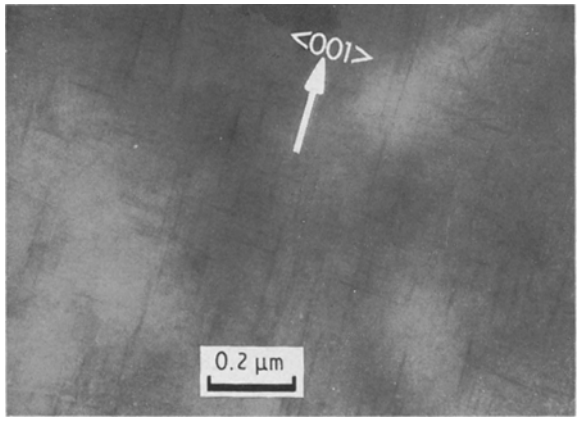

Figure 3 Bright-field transmission electron micrograph showing S laths in 8090. $B = \langle 0\,0\,1 \rangle$.

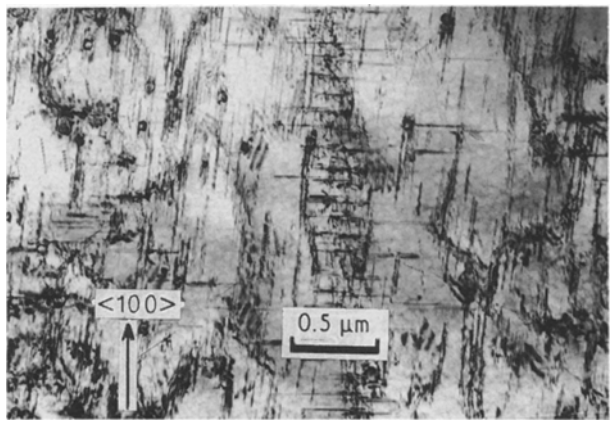

Figure 4 Bright-field transmission electron micrograph showing S laths on a sub-boundary in 8090. *B* close to ⟨1 1 0⟩.

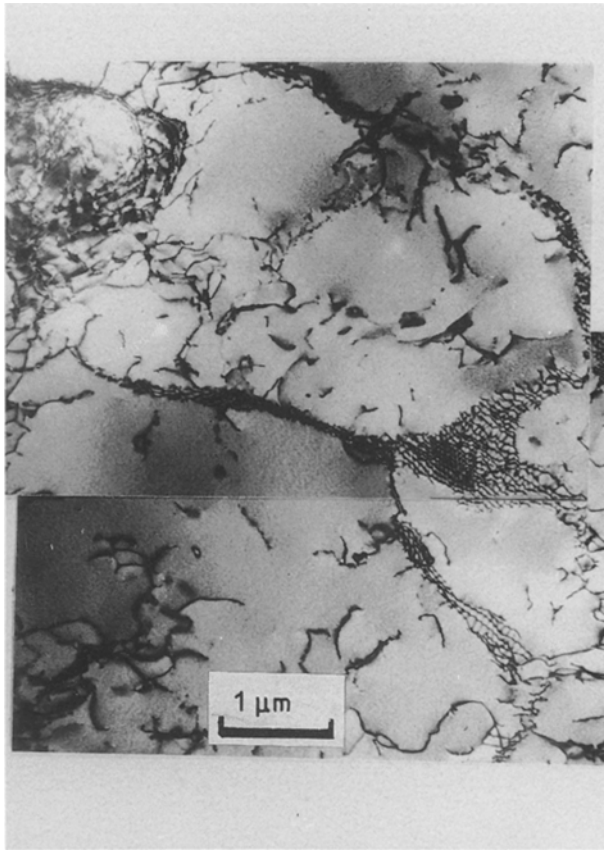

Figure 5 Bright-field transmission electron micrograph showing well-developed sub-grain structure in Al–0.95% Li solid solution crept to fracture at 40 MPa/423 K. $B = \langle 1\,0\,1 \rangle$.

to contain dislocation pairs which shear the δ′ particles (Fig. 7). The 2.75% Li binary alloy exhibits sub-grains which contain coarse δ′ particles which are heavily looped by dislocations (Fig. 8). Some of these dislocations may occur as a result of loss of coherency, but this is unlikely as δ′ is reported to remain coherent up to a size of 300 nm diameter [36], compared to the present size of 174 nm diameter. The 2090 alloy contains δ′ and T_1 within sub-grains formed initially during hot working before creep testing. The average size of the δ′ increases during creep up to a maximum of 5 nm diameter: Single dislocations and dislocation pairs are seen (Fig. 9a) with dislocations observed to

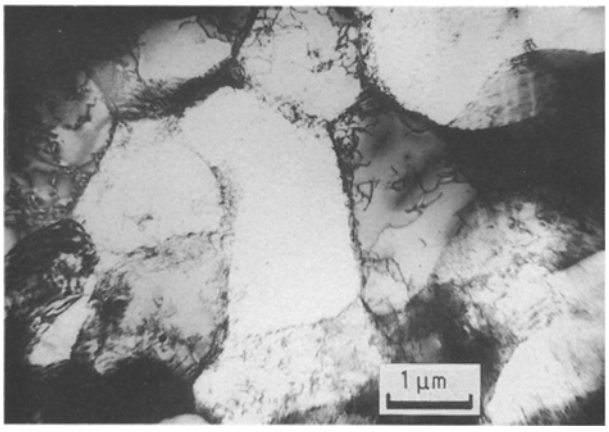

Figure 6 Bright-field transmission electron micrograph showing well-developed sub-grain structure in Al–1.94% Li alloy. $B = \langle 1\,0\,1 \rangle$.

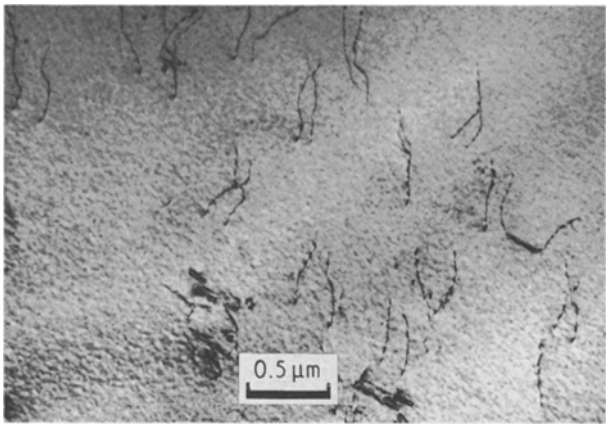

Figure 7 Bright-field transmission electron micrograph showing dislocation pairs in Al–1.94% Li alloy crept to fracture at 100 MPa/423 K. $B = \langle 0\,0\,1 \rangle$.

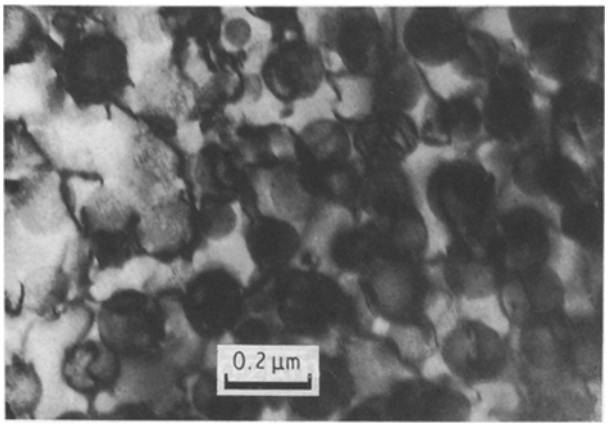

Figure 8 Bright-field transmission electron micrograph showing Orowan loops in Al–2.75% Li alloy crept to fracture at 142 MPa/423 K. $B = \langle 1\,0\,1 \rangle$.

loop or wrap around T_1 plates (Fig. 9b). The 8090 alloy contains δ′ within sub-grains, formed initially during hot working, and S both within sub-grains and on sub-grain boundaries. The δ′ particle size increases during creep up to a maximum diameter of 32 nm with the volume fraction increasing from 0.05 to 0.08. The S laths grow to a maximum length of 300 nm and the

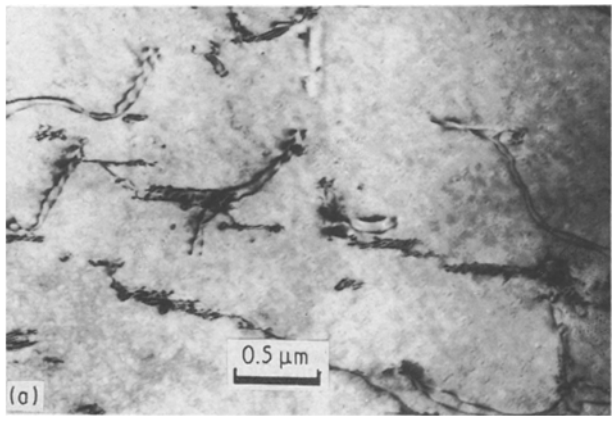

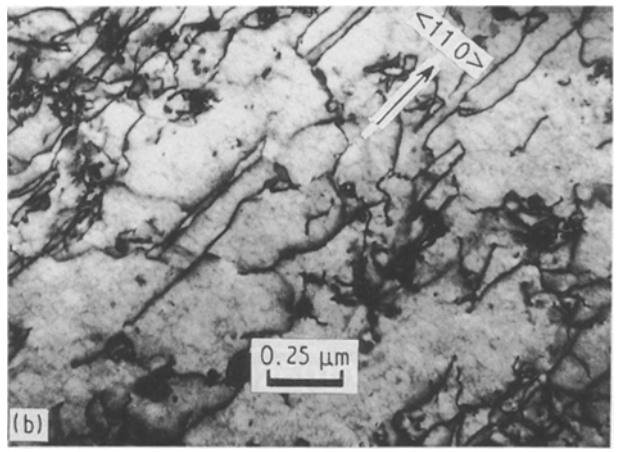

Figure 9 Bright-field transmission electron micrographs showing (a) single dislocations and dislocation pairs in 2090 crept to fracture at 250 MPa/423 K, $B = \langle 1\,0\,1 \rangle$ and (b) dislocations wrapping around T_1 plates in 2090 crept at 250 MPa/423 K, $B = \langle 1\,0\,1 \rangle$.

volume fraction increases from 0.01 to 0.05 within the sub-grains, during creep. Further precipitation of S takes place on dislocations in sub-grain boundaries and on some dislocations within sub-grains. Dislocation pairs, bowing dislocations and dislocation loops are seen (Fig. 10). It is not clear whether the loops are only around S or whether some are around δ′.

3.3. Internal stress

The internal stress, σ_i, has been measured in crept specimens of Al–2.75% Li, 2090 and 8090 [9] using the strain transient dip test [9, 10]. The results are given in Fig. 11 as a function of the applied creep stress, σ_a. For the 2090 and 8090 alloys, σ_i is seen to increase linearly with applied stress until it becomes approximately constant at a given maximum applied stress. The magnitudes of the internal stress are clearly very different. For the binary alloy the internal stress varies little with the applied stress, in the range studied, although σ_i seems to decrease at the lowest applied stress.

The internal stress develops as a result of inhomogeneities of plastic deformation and will always increase with the extent of plastic strain until the stresses developed are of sufficient magnitude to initiate processes which relax this stress or at least prevent it from increasing. The main dislocation configurations which

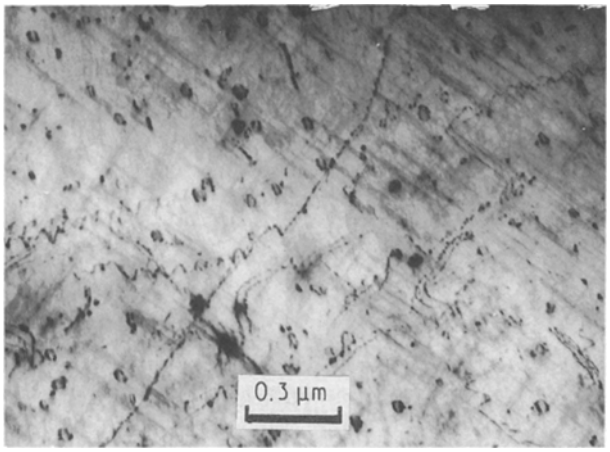

Figure 10 Bright-field transmission electron micrograph showing dislocation loops, dislocation pairs and bowing dislocations in 8090 crept to fracture at 375 MPa/423 K. $B = \langle 001 \rangle$.

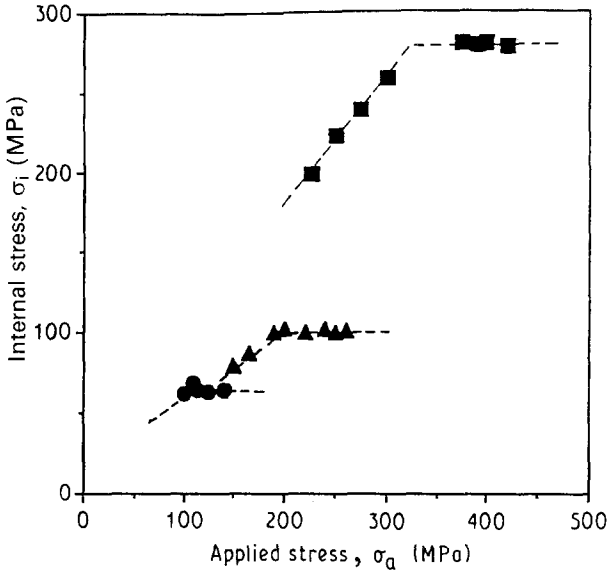

Figure 11 Internal stress as a function of applied stress for (●) Al–2.75% Li, (▲) 2090 and (■) 8090, at 423 K.

result in internal stresses are well-developed dislocation sub-boundaries [37–44] and Orowan loops around second-phase particles [5, 6]. In the present alloys, both such configurations are observed.

In pure aluminium and dilute aluminium alloys, crept specimens containing well-developed dislocation sub-boundaries, exhibited internal stresses which increased with increasing applied creep stress [37, 40, 41, 44, 45]. In nickel-based alloys, containing no sub-boundaries, but relatively coarse γ' particles, the internal stress increases with applied creep stress but becomes approximately constant at high stresses [1–6]. In the case of Nimonic 91 [5, 6], containing no sub-boundaries, it was possible to show that a significant proportion of the mechanically measured internal stress could be accounted for by the measured number of γ' particles which were Orowan looped. In the present case, σ_i increased with applied stress for 8090 and 2090, becoming approximately constant at high stresses, at $\sigma_i/\sigma_a \approx 0.52$ for 2090, $\sigma_i/\sigma_a = 0.9$ for 8090 and $\sigma_i/\sigma_a = 0.65$ for Al–2.75% Li. Clearly the internal stress in these alloys will depend on both the contribution of the sub-boundaries and the contribution from Orowan loops around particles.

In the case of Al–2.75% Li, loops and bowing dislocations were always seen around the coarse δ' particles. At a creep stress of 100 MPa, nearly every particle seems to have at least one loop around it. The internal stress that these loops would generate [5, 6] is given by

$$\sigma_i = (3/2) f_L G n b / \bar{r} \quad (5)$$

where n is the number of loops around a particle of mean radius $\bar{r}$ and f_L is the volume fraction of looped particles. Using $f_L = f = 0.22$ and $n = 1$ yields an internal stress of 32 MPa compared to the measured value of 70 MPa. It must be emphasized that this is only a rough estimate, as detailed counting of loop numbers has not been carried out, as it was for Nimonic 91 [5, 6]. Nevertheless, it suggests that a significant contribution to σ_i originates from Orowan loops but an equally significant contribution must come from the hard sub-boundaries. σ_i was determined for this material over a limited range of creep stresses near to or below the macroscopic yield stress (Table V, Fig. 11). Over this range, σ_i was approximately constant. If this is a genuine result, it may be due to an increased probability of particle shearing at higher stresses balancing an increasing sub-structure contribution.

The situation for the 8090 alloy is much more complex. The alloy contains lath-like S precipitate in the sub-grains and on sub-grain boundaries, as well as δ' in the sub-grains. The internal stress increases with applied stress up to the macroscopic yield stress (Table V, Fig. 11) and is then approximately constant at very high values of $\sigma_i = 280$ MPa or $\sigma_i/\sigma_a = 0.9$. The S precipitate must be Orowan looped but the fine δ' is probably not. The contribution of Orowan loops around S precipitate to the overall internal stress can be calculated in a similar manner to that previously utilized for γ' in Nimonic 91 [5, 6].

It is shown in the Appendix that the internal stress σ_i resulting from loops around S is given approximately by

$$\sigma_i = 6 G \varepsilon f_s \cos\theta \quad (6)$$

where ε is the plastic strain, f_s is the volume fraction of S and θ the angle between the S lath axis and the slip plane normal ($= 54.7°$). Taking the maximum volume fraction of S observed within the sub-grains of 0.005, then the internal stress after a strain of 0.02 would be $\sigma_i = 10$ MPa. This value is very small compared to the maximum measured value of 280 MPa and this is a direct consequence of the very small volume fraction of S. Even if all the δ' were looped, which is certainly not observed, then Equation 5 would give a value of σ_i of only 68.4 MPa for the highest volume fraction of δ' measured. In the case of 8090 then it is clear that although Orowan looping of S within sub-grains must occur during creep, it does not contribute significantly to the internal stress and looping of δ' would not be much more significant. Clearly the majority, by far, of the internal stress must arise as a result of the hard

TABLE V

	Li (%)				
	0.95 (3.57)	1.9 K (7.09)	2.75 (9.84)	2090 (7.25)	8090 (8.33)
Creep "yield stress" (MPa) at 423 K/150 °C	38	111	123	229	299

sub-boundaries. The magnitude of this contribution is very large compared to that of sub-boundaries in solid solution alloys. In the 8090 alloy sub-boundaries were present prior to creep and they are associated with hard β′ (Al_3Zr) particles, with some S laths precipitated on many of the dislocations. It is, in fact, this precipitation of S on sub-boundaries which has previously been suggested to be responsible for the observed very high stress dependence of the creep rate in 8090 [7]. These initial sub-boundaries are hence very hard and must deform plastically very little as the matrix deforms, resulting in large internal stresses in much the same manner as those arising due to non-deformable particles within sub-grains. The observed increase in internal stress with applied stress presumably results from the further accumulation of dislocations in the walls, due in part to the S precipitate barriers, more being accumulated at faster creep rates at higher stresses. At around the macroscopic yield stress (Table V, Fig. 11) the internal stress becomes approximately constant and at the same time long slip bands are seen traversing sub-boundaries. Clearly plastic deformation is becoming more homogeneous and furthermore the accumulation of dislocations in sub-grain walls ceases to increase with stress, i.e. the walls are yielding plastically with some of the sub-boundary S being sheared by dislocations. As a result the internal stress no longer increases or increases at a very much slower rate.

In the case of the 2090 alloy, the very fine δ′ is certainly sheared by dislocations but the T_1 plates must be Orowan looped as they cannot be easily sheared by $\{1\,1\,1\}\langle 1\,1\,0\rangle$ slip. Calculation of the resulting internal stress is not easy because the loops will be very far from having a circular shape but its magnitude must be proportional to the volume fraction of T_1 (approximately 2%) and be given very approximately by Equation 6. At a strain of 0.02 this would yield an approximate maximum value of 40 MPa compared to the maximum measured value of 100 MPa. The contribution to the internal stress from Orowan loops is hence likely to be of similar magnitude to, in this case, that from the relatively precipitate-free sub-boundaries. The measured internal stress increases with applied stress as the substructure develops with increasing stress but becomes constant at large applied stress. This again occurs at the macroscopic yield stress (Table V, Fig. 11) and may be due in part to the shear of T_1 by slip on $\{1\,0\,0\}$ or by twinning.

The measured internal stresses in these alloys hence results from both the looping of hard particles and from the presence of hard dislocation sub-boundaries. The contribution due to the looping of particles within sub-grains depends largely on the volume fraction of precipitate. The contribution is hence very small in the case of the 8090 alloy but is likely to be a significant fraction of the total in both 2090 and the Al–2.75% Li alloy. The aspect ratio of the particles is only significant in that spherical δ′ particles can be partly bypassed by climb or cross-slip during creep, unlike the long laths of S and plates of T_1. The accumulated Orowan looping of T_1 plates is hence likely to make a bigger contribution to the internal stress than the accumulated looping of spherical δ′ for a given volume fraction. The internal stresses developed due to sub-boundaries in 2090 and Al–2.75% Al are comparable to those due to Orowan looping. In 8090 precipitates of S on sub-boundaries significantly hardens them resulting in very large values of the internal stress. In both 2090 and 8090 the internal stress becomes approximately constant at stresses exceeding the macroscopic yield stress. This may result from yielding of sub-boundaries decorated with S in 8090 and yielding of T_1 plates in 2090.

3.4. Secondary creep

The creep curves for all the alloys showed a decelerating primary, a period of relatively constant creep rate in secondary and an accelerating creep rate in tertiary until fracture. Only the measured secondary creep rates will be discussed in this paper.

The secondary creep rate, $\dot{\varepsilon}$, for the 1% Li solid solution alloy is shown as a function of applied stress, σ_a, in Fig. 12. The results can be represented by the relationship $\dot{\varepsilon} \propto \sigma^n$ with the stress exponent n being 4.6. This stress exponent, together with the shape of the creep curve and the fact that well-developed sub-grains are observed during creep, suggests Class II behaviour with dislocation climb playing a significant role during creep. The creep rates are compared to those for pure aluminium [46] also plotted in Fig. 12. The slopes of the two plots are very similar with the creep rates for the 1 mass % Li solid solution being a factor of 4–5 slower at the same creep stress. These results are comparable to others for Al–Li solid solutions [35, 47] where stress exponents of 4.6 have been reported with the creep rate decreasing by a factor of 10 for a 2 mass % Li addition [43]. It has been suggested [35] that the decreased creep rate may be a result of a lower diffusion coefficient and/or lower stacking fault energy. These effects, while small, cannot be ignored in the precipitation-hardened alloys where the matrix contains approximately 1.5 mass % Li. The internal stress was not measured in this alloy

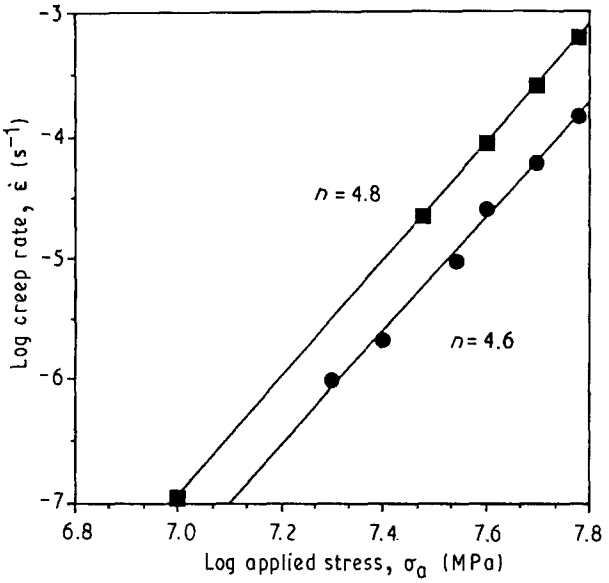

Figure 12 Log creep rate as a function of log applied stress for (●) Al–0.95% Li and (■) aluminium at 423 K.

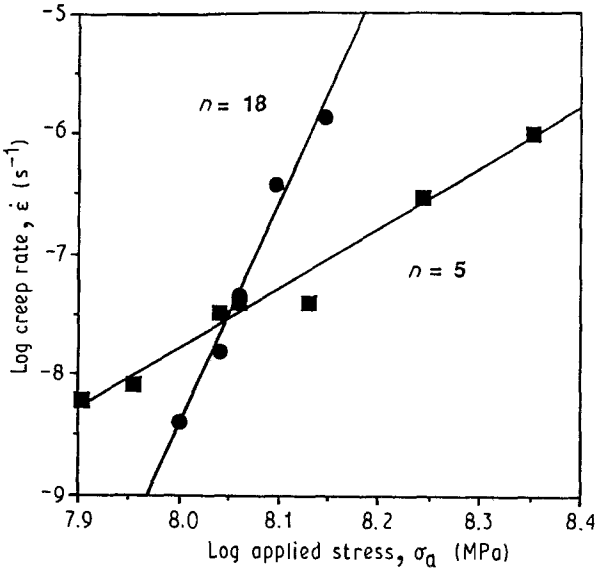

Figure 13 Log creep rate as a function of log applied stress for (■) Al–1.94% Li and (●) Al–2.75% Li, at 423 K.

but internal stresses are assumed to be present as a result of the sub-boundaries and to increase with increasing creep stress as has been observed for aluminium and other aluminium alloys [37, 40, 41, 43, 45].

The creep rates for the two binary alloys containing spherical δ′ particles are shown as a function of applied stress in Fig. 13. The 1.94 mass % Li alloy contains 4% by volume of δ′ of 25 nm diameter. The particles are always cut, at least at yield, by dislocations. The creep rates for a given applied stress are 10^5 slower than for the solid solution alloy with a not dissimilar mass % Li in the matrix. The stress dependence of the creep rate is approximately 5.0 compared to that for the solid solution alloy of 4.6 and pure aluminium of 4.8. Again the internal stress was not measured but must be present, as well-developed sub-boundaries are observed. If it is assumed to be of similar magnitude to the solid solution alloy and also assumed to increase with applied stress, then the differences in creep rates cannot be due to differences in internal stress, σ_i, and hence effective stress ($\sigma_a - \sigma_i$). If creep occurs by dislocations wiggling their way across slip planes, cutting some particles and climbing others, depending on the local particle size and spacing, then the creep rate will depend on the δ′ volume fraction and the particle size and spacing. In this respect, for a given volume fraction, smaller, hence larger numbers of particles will be more effective in slowing the creep rate. It is suggested then, that in this alloy, where particles can be cut by dislocations, that the major effect of the particles is not on the magnitude of the internal stress but directly on the rate at which dislocations can glide/climb across the slip plane.

The behaviour of the 2.75 mass % Li alloy, which contains very coarse δ′ of 174 nm diameter is very different. The stress dependence of the creep rate is very high with a stress exponent, n, of 18.3. This large stress dependence is a direct result of the internal stress being independent of applied stress, in the stress range studied, resulting in the effective stress ($\sigma_a - \sigma_i$) increasing rapidly with applied stress. In this alloy the coarse δ′ cannot be cut by dislocations, resulting in a high density of Orowan loops. This contribution of Orowan loops to the internal stress will certainly make the internal stress larger in this alloy, at least at low stresses, when compared to the Al–1.94% Li alloy where δ′ particles can be cut by dislocations. It may, however, be the case that at high stresses, the unimpeded development of dislocation substructure results in higher internal stresses in the Al–1.94% Li alloy. If this is the case, then the cross-over of the log σ versus log $\dot{\varepsilon}$ plots in Fig. 13 is largely the result of the constancy of internal stress in Al–2.75% Li and on internal stress which may continuously increase with applied stress for the Al–1.94% Li alloy, i.e. the cross-over is a result of differences in the effective stress for a given applied stress. The observed creep rates depend both on the magnitude of the effective stress and on the ease with which a dislocation can glide/climb its way across a slip plane. The Al–2.75% Li alloy contains a volume fraction of 0.23 δ′ of diameter 174 nm while the Al–1.94% Li alloy contains only a volume fraction of 0.04 of diameter 25 nm. Intuitively, it would be expected that a dislocation would have to climb less on its way across the glide plane to avoid the δ′ particles in the lower volume fraction alloy. The extent to which this is true will depend on the particle size distribution, as only the tail end of the distribution (i.e. smaller particles, larger spacings) will be sampled by dislocations during creep. Whatever is the case, the creep rates for a given applied stress are surprisingly similar for very different volume fraction alloys. In fact it would appear that the smaller particles are more effective in slowing the creep rate, albeit the effects on the creep rate arise from different sources for the two particle sizes.

The creep rates for the ternary and quaternary alloys are given as a function of applied stress in Fig. 14. The stress dependences of the creep rates at low stresses are given by $n = 4.8$ for 2090 and $n = 4.5$ for 8090. At high stresses stress exponents of $n = 14.7$

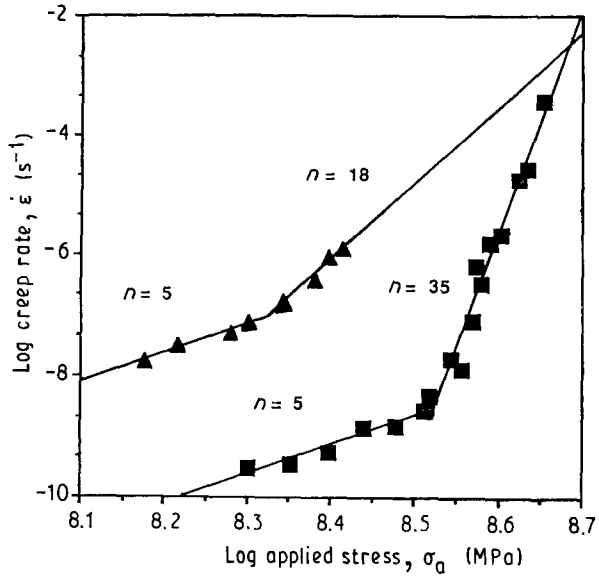

Figure 14 Log creep rate as a function of log applied stress for (▲) 2090 and (■) 8090, at 423 K.

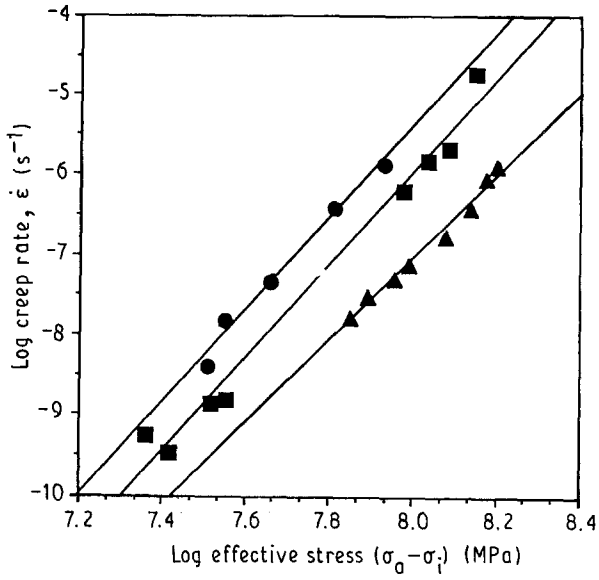

Figure 15 Log creep rate as a function of log effective stress for (●) Al–2.75% Li, (▲) 2090 and (■) 8090, at 423 K.

for 2090 and $n = 35$ for 8090 are observed. The change in the stress dependence occurs at the stress at which the measured internal stress becomes constant (Figs 11 and 14) which approximates to the macroscopic yield stress (Table V). The differences in the creep rates for a given applied stress are large, corresponding to the very large differences in the measured internal stresses. Clearly the precipitation of S on subgrain boundaries, hardening them, in the 8090 alloy, is a much more effective way of increasing the internal stress than the Orowan looping of T_1 plates in the matrix in the 2090 alloy. The creep rates as a function of effective stress ($\sigma_a - \sigma_i$) for the Al–2.75% Li, 2090 and 8090 alloys are shown in Fig. 15. The creep rates are given by

$$\dot{\varepsilon} \propto (\sigma_a - \sigma_i)^n \quad (7)$$

with the stress exponent n being 5–6 in all cases at all stresses. The extremes of differences in creep rate for a given applied stress are now only one order of magnitude. The major differences in creep rate hence arise from differences in the internal stress and hence effective stress, for a given applied stress. If it is assumed that in all three cases creep occurs by dislocations wiggling across glide planes by glide/climb, under the action of the effective stress, then the differences in creep rate between the three alloys must arise as a result of the relative ease of this process. All three alloys contain spherical δ′ particles but the binary alloy has by far the largest volume fraction. These particles, however, are easier for dislocations to circumvent by climb than the long laths of S and large plates of T_1 in the 8090 or 2090 alloys, respectively. These particles appear to be more efficient in slowing the creep rate at a given effective stress, with the higher volume fraction of T_1 decreasing the creep rate to the largest extent.

Finally, it is interesting to compare the creep rates of the Al–1.94% Li alloy with those of the 2090 alloy (Fig. 16). Both alloys contain similar volume fractions

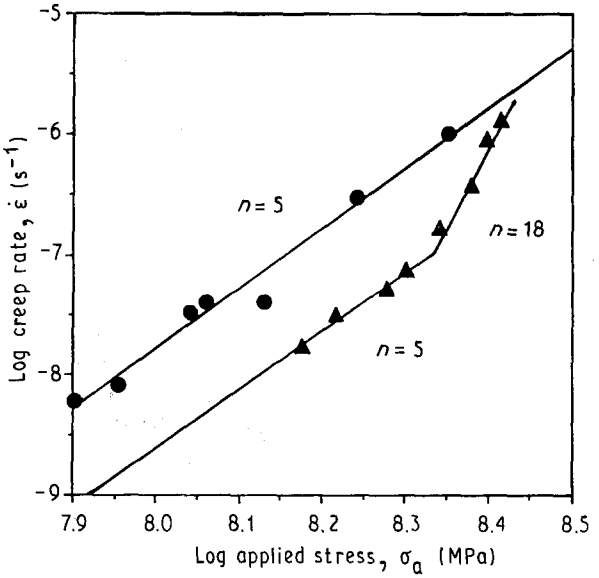

Figure 16 Log creep rate as a function of log applied stress for (●) Al–1.94% Li and (▲) 2090, at 423 K.

of δ′ of sizes such that they are cut by dislocations. In addition, the 2090 alloy contains large plates of T_1 which are not easily cut by dislocations. The presence of the T_1 plates which must be Orowan looped at all but the highest stresses, increases the internal stress and makes the glide/climb of dislocations more difficult. At low stresses then, both alloys have a similar stress dependence of the creep rate, but 2090 creeps more slowly. At larger stresses the stress dependence of the creep rate increases for 2090, as a result of the constancy of the internal stress, due to some possible shearing of T_1, and the creep rates converge.

4. Conclusion

The present work set out to investigate the effect of S, T_1 and δ′ precipitates on the internal stress and creep

of aluminium–lithium based alloys. In the solid solution alloy and Al–1.94% Li in which δ′ is easily sheared by dislocations, the stress dependence of the creep rate is that expected for Class II behaviour with a stress exponent n of 4–5. The internal stress in these alloys is assumed to be due to the presence of well-developed sub-boundaries and is assumed to increase with increasing applied stress. The presence of the δ′ particles markedly reduces the creep rate as the dislocations glide/climb across the glide plane, cutting some particles and climbing over others. It is now clear that it is the presence of coarse δ′, S and T_1 which are not easily sheared by dislocations which results in the high stress dependence of the creep rate at high applied stresses. It is suggested that the high stress dependence arises when these precipitates start to be sheared by dislocations resulting in an approximate constancy of internal stress with increasing applied stress. This results in an effective stress $(\sigma_a - \sigma_i)$ which changes rapidly with applied stress and a corresponding rapid change of creep rate with applied stress. In the case of Al–2.75% Li and 2090, it is the presence of Orowan loops around coarse δ′ and T_1, respectively, which contribute to the internal stress and it may be the shear of these at high stresses which leads to the constancy of the internal stress. In the case of 8090 it may be the hardening of sub-boundaries by the precipitation of S on boundary dislocations which leads to the very large internal stresses and the shear of these sub-boundary S precipitates which leads to the constancy of internal stress at high creep stresses.

If the creep rate is plotted as a function of the effective stress $(\sigma_a - \sigma_i)$ for these alloys then a single stress exponent n of between 5 and 6 is found, i.e. $\dot{\varepsilon} \propto (\sigma_a - \sigma_i)^n$, at all stresses. At a given effective stress the creep rate is determined by the ease with which dislocations can glide/climb across the slip plane avoiding precipitate particles. In this respect the S laths and T_1 plates are more effective than the coarse spherical δ′ particles.

Acknowledgements

The authors thank Dr D. A. Granger, ALCOA Technical Center, USA, Dr R. Ricks Alcan International, UK, Dr D. S. McDarmaid, RAE Farnborough, UK, and Dr D. Talbot, Brunel University, UK, for supplying, and assistance with fabrication of, the alloys.

Appendix

Here an approximate expression for the internal stress arising from the formation of Orowan loops around S laths is derived. It is assumed that S must be looped and cannot be cut. Because of the geometry of S, bypassing by climb or cross-slip and relaxation mechanisms such as prismatic punching are not possible.

The tensile strain, ε, can be written as

$$\varepsilon = b \sum m_i A_i \qquad \text{(A1)}$$

where b is the magnitude of the Burgers vector, m_i is the orientation factor for slip system i and A_i is the area swept out per unit volume by all dislocations of this system.

Using the Taylor value of 1/3 for the average value of m, the total area swept out per unit volume is

$$A = \frac{3\varepsilon}{b} \qquad \text{(A2)}$$

The area fraction of S in a (1 1 1) section is f_s (volume fraction and area fraction are identical) hence the area of S per unit volume which must be looped is $3f_s\varepsilon/b$. If this is divided by the mean area of an S lath in a (1 1 1) section, the number, N_L, of loops per unit volume is found. If a is the normal cross-sectional area of S, the area on the (1 1 1) plane is $a/\cos\theta$ where θ is the angle between the lath axis (⟨1 0 0⟩) and the normal to {1 1 1} (θ = 54.7°). Thus

$$N_L = \frac{3f_s\varepsilon\cos\theta}{ab} \qquad \text{(A3)}$$

It is now assumed that each Orowan loop of radius r generates the same internal stress as it would if it surrounded a spherical particle of radius r. Equation 5 can be written in terms of the number of loops per volume as

$$\sigma_i = 2\pi N_L G b \left(\frac{\overline{r^3}}{\bar{r}}\right) \qquad \text{(A4)}$$

and using Equation A3 this gives

$$\sigma_i = 6\pi G\varepsilon f_s \cos\theta \left(\frac{\overline{r^3}}{\bar{r}a}\right) \qquad \text{(A5)}$$

The quantity $\overline{r^3}/(\bar{r}a)$ is clearly a number of order $1/\pi$ and hence

$$\sigma_i \approx 6G\varepsilon f_s \cos\theta \qquad \text{(A6)}$$

The internal stress is therefore proportional to the volume fraction of precipitate and to the strain but independent of the loop size.

References

1. K. R. WILLIAMS and B. WILSHIRE, *Met. Sci. J.* **7** (1973) 176.
2. W. J. EVANS and G. F. HARRISON, *ibid.* **10** (1976) 307.
3. H. BURT, J. P. DENNISON and B. WILSHIRE, *ibid.* **13** (1979) 295.
4. R. A. STEVENS and P. E. J. FLEWITT, *Acta Metall.* **29** (1981) 867.
5. C. K. L. DAVIES, A. G. OLDER and R. N. STEVENS, in "Proceedings of the 4th International Conference on Creep and Fracture of Engineering Materials and Structures", Swansea, UK, edited by R. W. Evans and B. Wilshire (Institute of Metals, London, 1990) pp. 97–107.
6. *Idem, J. Mater. Sci.* to be published.
7. S. J. HARRIS, B. NOBLE, K. DINSDALE and M. PRIDHAM, in "Aluminium Alloys: Their Physical and Mechanical Properties", Conference, Charlottesville, Virginia, USA (1986), Vol. 2, p. 755.
8. M. HAYASHI and H. OIKAWA, *J. Jpn Inst. Light Metals* **36** (1986) 768.
9. C. K. L. DAVIES, S. POOLAY-MOOTIEN, R. N. STEVENS and P. L. TETLOW, *J. Mater. Sci.* to be published.
10. J. C. GIBELING and W. D. NIX, *Mater. Sci. Engng* **45** (1980) 123.
11. Y. MIURA, K. YUSU, S. AIBE, M. FURUKAWA and M. NEMOTO, in "5th Al–Li Conference", Williamsburg, VA edited by T. H. Sanders and E. A. Starke (MCE, 1989) p. 827.

12. P. L. TETLOW, PhD thesis, Queen Mary and Westfield College, University of London (1991) p. 239.
13. P. M. KELLY, A. JOSTSONS, R. G. BLAKE and J. G. NAPIER, *Phys. Status Solidi.* **31a** (1975) 771.
14. C. K. L. DAVIES and R. N. STEVENS, unpublished work.
15. S. CERESARA, G. COCCO, G. FAGHERAZZI and L. SCHIFFINI, *Phil. Mag.* **35** (1977) 373.
16. Y. MIURA, A. MATSUI, M. FURUKAWA and M. NEMOTO, in "Proceedings of the 3rd International Conference on Al–Li Alloys", Oxford, UK, edited by C. Baker, P. J. Gregson, J. S. Harris and C. J. Peel (Institute of Metals, London, 1986) pp. 427–34.
17. L. M. BROWN and R. K. HAM, in "Strengthening Methods in Crystals", edited by A. Kelly and R. B. Nicholson (Applied Science, London, 1971) Ch. 2, p. 9.
18. J. C. HUANG and A. J. ARDELL, *Acta Metall.* **36** (1988) 2995.
19. W. A. CASSADA, G. J. SHIFLET and E. A. STARKE Jr, *ibid.* **34** (1986) 367.
20. J. C. HUANG and A. J. ARDELL, *Mater. Sci. Engng* **A104** (1988) 149.
21. B. NOBLE, S. J. HARRIS and K. DINSDALE, *J. Mater. Sci.* **17** (1982) 461.
22. M. TAMURA, T. MORI and T. NAKAMURA, *Trans. Jpn Inst. Metals* **14** (1973) 355.
23. W. MULLER, E. BUBECK and V. GEROLD, in "Proceedings of the 3rd International Conference on Al–Li Alloys", Oxford, UK, edited by C. Baker, P. J. Gregson, S. J. Harris and C. J. Peel (Institute of Metals, London, 1986) p. 435.
24. P. SAINFORT and P. GUYOT, in "Proceedings of the 7th International Conference on the Strength of Metals and Alloys", Montreal, Vol. 1, edited by H. J. McQueen, J. P. Bailon, J. I. Dickson, J. J. Jonas and M. G. Akben (Pergamon, Oxford, 1985) p. 441.
25. M. FURUKAWA, Y. MIURA and M. NEMOTO, *Trans. Jpn Inst. Metals* **26** (1985) 230.
26. S. NOBLE, S. J. HARRIS and K. DINSDALE, *Met. Sci.* **16** (1982) 425.
27. J. C. HUANG and A. J. ARDELL, in "Proceedings of the 3rd International Conference on Al–Li Alloys", Oxford, UK, 1985, edited by C. Baker, P. J. Gregson, J. S. Harris and C. J. Peel (Institute of Metals, London, 1986) pp. 455–70.
28. P. SAINFORT, PhD thesis, University of Grenoble, France (1985).
29. W. A. CASSADA, G. J. SHIFLET and E. A. STARKE Jr, *Metall. Trans.* **22A** (1991) 287.
30. *Idem, ibid.* **22A** (1991) 299.
31. R. J. RIOJA and E. A. LUDWICZAK, in "Proceedings of the 3rd International Conference on Al–Li Alloys", Oxford, UK, 1985, edited by C. Baker, P. J. Gregson, J. S. Harris and C. J. Peel (Institute of Metals, London, 1986) pp. 471–82.
32. A. K. MUKHERJEE, J. E. BIRD and J. E. DORN, *Trans. Amer. Soc. Metals* **62** (1969) 155.
33. P. YAVARI, F. A. MOHAMED and T. G. LANGDON, *Acta Metall.* **20** (1981) 1495.
34. M. S. SOLIMAN and F. A. MOHAMED, *Mater. Sci. Engng* **55** (1982) 111.
35. KYUNG-TAE PARK, ENRIQUE J. LAVERNIA and FARGHALLI A. MOHAMED, *Acta Metall.* **38** (1990) 1837.
36. D. B. WILLIAMS, in "1st Al–Li Conference Proceedings", Stone Mountain, Georgia, USA, 1980, edited by T. H. Sanders and E. A. Starke, (AIME, 1981) p. 89.
37. S. TAKEUCHI and A. S. ARGON, *J. Mater. Sci.* **11** (1976) 1542.
38. W. BLUM, *Z. Metallkde.* **678** (1977) 484.
39. W. D. NIX and B. ILSCHNER, in "5th International Conference on Strength of Metals and Alloys", Aachen, edited by P. Haasen, V. Gerold and G. Kostorz (Pergamon Press, Oxford, 1979) p. 1503.
40. K. TOMA, H. YOSHINAGA and S. MORUZUMI, *Trans. Jpn Inst. Metals* **17** (1976) 102.
41. F. DOBES, *Acta Metall.* **28** (1980) 377.
42. H. MUGHRABI, *ibid.* **31** (1983) 1367.
43. D. CAILLARD, *Mater. Sci. Engng* **81** (1986) 349.
44. W. BLUM and E. WECKERT, *ibid.* **86** (1987) 145.
45. J. D. PARKER and B. WILSHIRE, *Phil. Mag. A* **41** (1980) 665.
46. D. McLEAN, *J. Inst. Metals* **81** (1952-3) 133.
47. M. NIIKURA, K. TAKAHASHI and C. OUCHI, in "Proceedings of the Third International Conference on Aluminium–Lithium Alloys", Oxford, UK, 1985, edited by C. Baker, P. J. Gregson, S. J. Harris and C. J. Peel (Institute of Metals, London, 1986) p. 213.

Received 16 October 1991
and accepted 23 January 1992